2023-01-1665

Ensemble Empirical Mode Decomposition for Characterising Exhaust Nano-Scale Particle Emissions of a Turbocharged Gasoline Power Unit

Ismail El Yacoubi
Stephen Samuel

Oxford Brookes University

Abstract

This paper presents a method for analysing the characteristics of nano-scale particles emitted from a 1.6 Litre, 4-stroke, gasoline direct injection (GDI) and turbocharged spark ignition engine fitted with a three-way catalytic converter. Ensemble Empirical Mode Decomposition (EEMD) is employed in this work to decompose the nano-scale particle size spectrums obtained using a differential mobility spectrometer (DMS) into Intrinsic Mode Functions (IMF). Fast Fourier Transform (FFT) is then applied to each IMF to compute its frequency content.

The results show a strong correlation between the IMFs of specific particle ranges and the IMFs of the total particle count at various speed and load operating conditions. Hence, it is possible to characterise the influence of specific nano-scale particle ranges on the total particulate matter signal by analysing the frequency components of its IMFs using the EEMD-FFT method. This approach can provide a useful insight for developing a control strategy for reducing nano-scale particle emissions of a GDI engine. The present work details the systematic methodology followed for using EEMD in combination with FFT to analyse the spectrums of nano-scale particulate matter emissions.

Introduction

Particulate Matter

Ever since the adverse health impact of nano-scale particulate matter (PM) from gasoline engines was identified, a significant amount of research was directed towards reducing the levels of PM from gasoline combustion sources. Most of the research work can be grouped into five main categories; (1) Formation mechanisms related to the operating conditions of the engine [1,2,3], (2) the characterisation of nano-scale particulate matter from gasoline direct injection (GDI) engines [2,3], (3) formation mechanisms linked to the chemical signature of fuels, lubricants, and other additives [4,5], (4) the measurement methods and uncertainties for meeting legislative emission targets [6] and finally (5) the after-treatment systems such as Gasoline particulate filters (GPF) [7].

Understanding the formation mechanism or size of soot particles during the combustion process is not a new area of research [8,9,10]. However, recent developments in measurement methodology, instrumentation [11,12] and research linking particulate matter with health risks [13] have enabled legislators to set up targets and researchers to develop strategies for controlling the formation mechanism and total PM quantity resulting from the combustion process. The mechanisms driving the creation of particles from fuel molecules during combustion were extensively studied along with the oxidation and particle growth mechanisms. For example, early studies proposed the presence of a link between unsaturated hydrocarbons such as polycyclic aromatic hydrocarbons (PAH) and airborne particulate matter formation [5]. The growth model reviewed by Richter and Howard [5] highlighted the effect of C_2 and C_3 units on the growth of molecules such as Benzene which results in the formation of larger PAH. Other pathways of PAH formation were also studied by Frenklach and Warnatz [14] who suggested a potential relation between the cyclization of cyclopentadienyl radicals and phenylacetylene formation. Melius et al. [15] later followed up on Frenklach and Warnatzs work and performed a quantum chemical analysis to test their hypothesis. The results of Melius et al. [15] confirmed the significant contribution of cyclopentadienyl radicals in the formation of aromatic rings, which are part of the particles nucleation process. The focus of the previously mentioned early studies was mainly related to diesel combustion. However, the general mechanism is not different for other petrochemical derived fuels. These studies also suggested that the smallest recognizable particles are in a range of less than 2 nm in diameter. In the next stage of particle formation, these particles grow, oxidise and coagulate based on the present fuel species and prevalent conditions such as temperature and pressure during the combustion process [16]. This stage of formation is mainly responsible for different particle size ranges for the given operating conditions. The growth of nanoparticles has been to a large extent expressed as variations of H-abstraction and C_2H_2-addition sequences [5]. For example, Nicovich and Ravishankara [17] used kinetic modelling as a method to analyse the products of the reaction $H + C_6H_6$. Their results demonstrated that cyclohexadienyl radical was formed by this reaction. The findings of their work were still valid even at sup-atmospheric pressures. Whereas Mebel et al. [18] conducted a study on reactions $H + C_6H_6$ and $C_6H_5 + H_2$, their results showed that reaction $H + C_6H_6$ had a significant dependence on pressure when temperature conditions are above room temperature.

Controlling the total count of nanoscale particles from gasoline-fuelled engines warranted insight from at least two specific areas. The first area of investigation focussed on the characterisation of the particles from gasoline combustion linked to the operating conditions of the engine. The second one focussed on the role of the chemical composition of gasoline and the affinity of certain species towards soot formation. Vehicle manufacturers and researchers broadly developed calibration procedures and control strategies for meeting PM emission

targets either in g/km or total particle count N#/km below the 1000 nm diameter range [3,6,19,20]. Various operating parameters related to event control such as fuel injection timing [21], spark timing [22], valve timing [23] and combustion duration along with design variables such as injector design, combustion chamber design and other combustion parameters [24] specifically related to inception, formation, growth and size distribution nano-scale particles are considered with the sole aim of meeting the emission targets [1].

Similarly, the chemical composition of fuel and its role in the formation, growth and size distribution of nano-scale particles was also studied by fuel chemists and researchers. The importance of this factor is recognised by legislators given the current regulations restricting sulphur content in diesel and gasoline fuel [25,26,27]. However, the precise mechanism that controls the inception, growth, fragmentation, coagulation and aggregation of nano-scale particles from gasoline fuel is not fully understood mainly because the measurements are carried after the combustion process. The size distribution is already frozen at this stage. Therefore, analysis work on the chemical composition of the exhaust gas, size distribution of nano-scale particles and the chemical composition of solid particles using methods such as thermo-gravimetric analysis [28] and Transmission Electron Microscopy [29] has been carried out by researchers. These studies took into consideration the engine operating conditions, the chemical composition of lubricating oil [30], different types of fuel additives along with their role on exhaust particles and the overall chemical composition of fuels [4].

In addition to gaining insight into the formation mechanisms and the effect of fuel chemical compositions on nano-scale particles, the variability, robustness and repeatability of PM measurements posed significant challenges to the legislators for setting total particle count target limits from gasoline engines [31,32]. Therefore, the Particle Measurement Programme at the European Commission [32] suggested different levels of counting efficiency for different particle size ranges based on experimental work. The effects on measurements repeatability can be linked to the cyclic variability of the combustion process [24], the dilution ratio set for the measurements [32] and the location of sampling positions such as pre and post catalyst, as well as pre and post turbocharger [33,34]. These variables have been shown to influence particle size characteristics even at steady-state operating conditions. So far, experimental observations have enabled researchers to only develop limited levels of correlation between different particle size ranges. Therefore, there is a need for developing appropriate models which can be used for gaining insight into the interactions between different particle size ranges. This will provide a clearer input definition to after-treatment systems such as gasoline particulate filters for controlling the PM emission levels.

In order to meet PM targets for gasoline engines, vehicle manufacturers developed gasoline particulate filters as an after-treatment solution. To evaluate and optimise the performance of this filter, the size distribution of the particles along with the total particle counts are required [35]. It is already known that the size distribution of the particles and total count upstream of the GPF vary from that of engine out PM levels since systems such as turbochargers and three-way-catalytic converters change the characteristics of nano-scale particles emitted from the combustion chamber [24,33,34,36,37]. Although reasonably strong experimental observations are available in the published literature, very limited mathematical methods predicting the influence of different exhaust subsystems on the size distribution and the total count of nano-scale particles are derived from these experimental observations [38].

It can be summarised that for any given operating conditions, various factors such as the coolant temperature, spark timing, injection pressure [39] and the start of injection timing have been shown to influence the formation mechanism of nano-scale particles [1,2,40]. Therefore, the size range of the particles and the total particle count can be controlled by optimising these parameters. For a given engine and fuel composition, the engine operating variables determine the total PM count as well as the size distribution of nano-scale particulate matter. For example, one of the control variables for a given air-fuel ratio and engine loading conditions explored by various researchers is the start of injection in gasoline engines [19,41,42]. This variable seems to influence the particle size distribution as well as the total particle count. In addition to that, the location of sampling points such as pre-catalyst or post-catalyst is also shown to have a significant influence on particle size distribution as well as the total particle count. Whereas regardless of sampling location, the correlation between the size distribution and the total particle count is essential for developing an appropriate control strategy [24,42,43]. However, very little literature on underpinning correlations between specific particle size ranges and the total particle count is found in the published domain. Hence, the scope of the present work. This study proposes the use of Ensemble Empirical Mode Decomposition (EEMD) as an approach for investigating the correlation between specific nano-scale particle size ranges and the total particle count.

Ensemble Empirical Mode Decomposition

Ensemble Empirical Mode Decomposition (EEMD) is a signal post-processing method introduced by Wu and Huang [44] and utilised for time domain data analysis. The suitability of this method for complex signal analysis is attributable to its adaptive features, ability to process non-stationary and non-linear datasets, as well as its ability to preserve time information during decomposition [44]. The process of employing EEMD consists of decomposing the input dataset into a set of Intrinsic Mode Functions (IMF) in addition to a residual. The purpose of this decomposition is to isolate multiple signal components within the data into separate IMFs, which allows a better understanding and extraction of physical meanings within the data. An IMF must satisfy two main requirements. The first requirement is that the number of times the signal crosses the horizontal axis must be the same or different by one to the number of extrema within the signal. Secondly, the mean of the local maxima and minima envelopes must be zero at any point in the dataset [45].

EEMD was presented as a noise-assisted data analysis (NADA) approach and provides a solution to the mode mixing problem associated with the original Empirical Mode Decomposition (EMD) algorithm published by Huang et al. [46] in 1998. Mode mixing occurs when one or more resulting IMFs contain multiple oscillations with varying scales. This means that the physical events associated with certain oscillations are not adequately represented in mode mixing affected IMFs, which can lead to the loss of some signal features present in the original dataset. EEMD overcomes this issue by adding white noise to the input signal. The added noise is utilised as a uniform reference during the decomposition process and therefore significantly reduces the likelihood of mode mixing. The added noise is cancelled out during the IMFs last mean computation [44, 45]. The process

followed for computing IMFs using EEMD is commonly known as the shifting algorithm [46]. For a signal given as *y(t)*, Huang et al. [46] defined the shifting algorithm steps followed during the EEMD process as the following:

1. Locate the local extrema (Minima & Maxima) of the input dataset *y(t)*.
2. Perform an interpolation of the local extrema by employing the cubic spline approach and find the upper and lower envelopes (*U(t)* & *L(t)*).
3. Compute the local mean (*m(t)*) of the upper and lower envelopes: $m_1(t) = \frac{U(t)+ L(t)}{2}$
4. Perform a subtraction of $m_1(t)$ from the input dataset: $j_1(t) = y(t) - m_1(t)$
5. Repeat steps 1 to 4 for $j_1(t)$ until reaching a $j_n(t)$ that meets the two conditions of an IMF.

The residual *r(t)* is generated once the remaining signal component after the last computed IMF is a monotonic function. Therefore, equation 1 can be used to reconstruct the original dataset:

$$y(t) = \sum_{k=1}^{k-1} IMF_k(t) + r(t) \quad (1)$$

To illustrate a practical application of the EEMD concept, signal *y(t)* shown in figure 1 was generated. The main components of this signal are three sinusoidal waves with frequencies of 10 Hz, 30 Hz and 70 Hz. Random noise was added to the signal to assess its effect on the results of the data decomposition. The resulting IMFs of signal *y(t)* are illustrated in figure 2. Fast Fourier Transform (FFT) was then applied to the IMFs to analyse their frequency content. It can be seen from figure 3 that the 70 Hz, 30 Hz and 10 Hz signal components are captured in IMFs 3, 4 and 5, respectively. Therefore, it is possible to separate critical signal features within a complex signal using EEMD.

EEMD was previously utilised for various applications in signal post processing and feature extraction. For example, Wang and Shao [47] used EEMD as a tool to extract fault features within the vibration signal of rotating machinery. Similarly, a paper published by Park, Kim and Choi [48] proposed an approach for gearbox fault diagnosis based on EEMD. Their method consists of decomposing the gearbox transmission error signal into a set of IMFs using EEMD. This facilitates detecting the difference between the faulty and normal gearbox by analysing the features within each IMF. Whereas El Yacoubi and Samuel [49] decomposed cylinder pressure data of a GDI engine using EEMD and showed that it is possible to identify engine firing features within the IMFs by analysing the frequency domain of each IMF. A similar approach is employed in the present work by decomposing the measured PM data using EEMD. FFT is then applied to the resulting IMFs to analyse its frequency features.

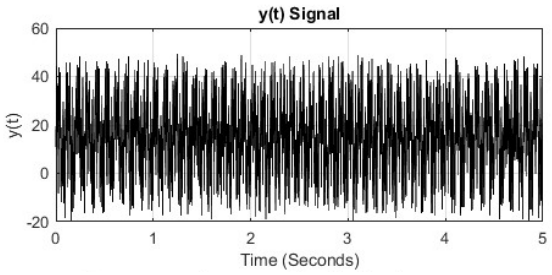

Figure 1: Graphical representation of the example signal *y(t)*

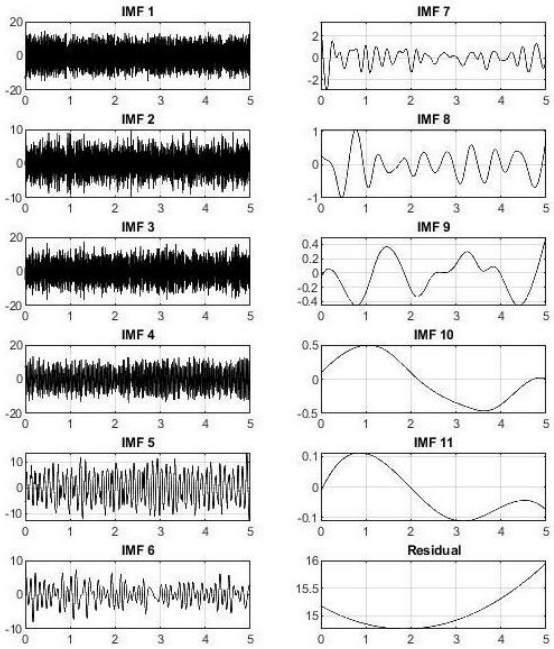

Figure 2: Resulting IMFs after applying EEMD to signal y(t)

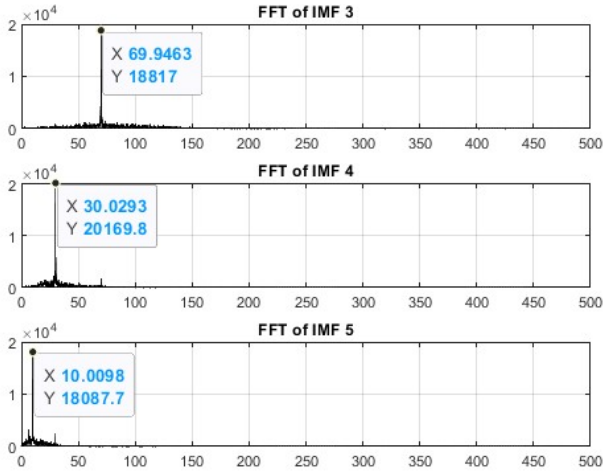

Figure 3: Frequency domain of IMFs 3, 4 and 5 of signal y(t)

Experimental apparatus

Power unit

The experimental data collected during this work are from a 1.6 Litre, 4-stroke, gasoline direct injection (GDI) and turbocharged spark ignition engine fitted with a three-way catalytic converter. Additional specifications of the test engine are shown in table 1.

The wall-guided direct injection (WGDI) strategy of the test engine consists of injecting fuel into the cylinder via a swirl injector installed on the side of the cylinder. The injector setup combined with a bowl-shaped pocket design of the piston crown allows easier guidance of the air-fuel mixture towards the spark plug. The test engine has a maximum fuel injection pressure of 12 MPa. This pressure level allows for a higher spray velocity compared to the piston velocity [10]. The engine control unit (ECU) modulates fuel injection pressure based on speed and load operating conditions to ensure optimum fuel consumption and emissions levels. The WGDI along with injection pressure specifications based on the operating conditions of the test engine play a crucial role in reducing fuel impingement on the cylinder walls. This is an important PM experimental testing consideration given the direct link between particle emissions and fuel injection parameters of GDI engines [50,51,52]. Elevated levels of wall fuel impingement often result in an alteration in fuel evaporation dynamics and therefore lead to a significant change in the characteristics of PM emissions [37,53].

Particulate matter measuring device

The present work utilises a Differential Mobility Spectrometer DMS-500 as a device to sample particulate matter data from the exhaust gas. This device is capable of measuring PM total count and size spectrums for particles with a geometric mean diameter (GMD) between 5 nm and 1000 nm. The sampling period used to collect PM measurements was 500 milliseconds.

Table 1: Experimental engine specifications

Parameter	Value
Peak torque	240 Nm @ 4000 RPM
Rated power	130 kW @ 6000 RPM
Bore diameter	77 mm
Stroke length	85.8 mm
Connecting rod length	138.4 mm
Number of cylinders	4
Compression ratio	10.5
Pistons firing order	1 – 3 – 4 – 2
Fuel injection type	Gasoline Direct injection
Induction type	Turbocharged and intercooled

Methodology of work

Experimental testing

Particulate matter data used in this work were collected from the test engine at fully warmed-up and steady-state operating conditions. An eddy current dynamometer controlled by a CADET V12 system was utilised to maintain the desired engine speed and load inputs within ± 2 RPM and ± 1 Nm, respectively. This ensures higher accuracy in steady-state measurements. The collected steady-state conditions in the present work are 1500 RPM at 50 Nm, 1500 RPM at 80 Nm, 2500 RPM at 20 Nm, 2500 RPM at 50 Nm, 3500 RPM at 20 Nm and 3500 RPM at 80 Nm. Oil and coolant temperatures during the experiment were recorded as 89 °C and 83 °C, respectively. These temperature readings were taken after a full 20 minutes of engine warm-up to allow for oil and coolant temperature stabilisation and ensure a non-fluctuating reading. Ambient air temperature is assumed to be 21 °C during the reading.

The exhaust samples were taken from upstream as well as downstream of the three-way catalytic converter. A heated selector valve maintained at 190 °C was used to allow for choosing a sampling location prior to or post catalyst. Figure 4 illustrates a schematic representation of the experimental setup.

The duration of PM emissions measurements was 10 mins for all operating conditions. This is to account for particle count variability and allow a better representation of frequency properties during the data post-processing stage.

Signal post-processing

The data analysis approach employed in the present work consists of applying EEMD to the particle count spectrums obtained experimentally at different operating conditions. The purpose of this approach is to obtain a set of Intrinsic Mode Functions representing various signal features for each test case. RStudio integrated development environment (IDE) for R© 4.2.2 was used for performing EEMD using the integrated Rlibeemd package.

Next, Fast Fourier Transform was applied to the IMFs obtained from EEMD to obtain the frequency characteristics of each IMF. The integrated FFT function within MATLAB programming software was used in this work to compute the frequency domain of the IMFs.

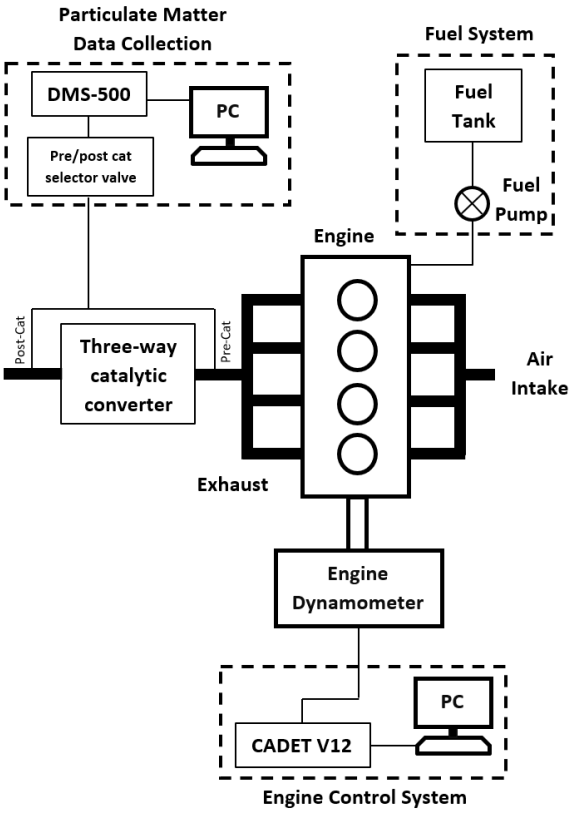

Figure 4: Schematic representation of the experimental setup used for PM data collection

Results and discussion

A typical particle spectral density for every 60 seconds as a function of particle diameter is shown in figure 5. It can be seen that the general trend of the particle spectral density is similar for every 60 seconds increment of the sampling duration. This is expected as the measurements were taken during steady-state operating conditions. However, it can also be seen that most of the fluctuation in particle spectral density from one 60 seconds increment to the next is within the 10 nm to 50 nm diameter region. This is also expected given that this nanoparticle range represents the majority of particulate matter emissions from gasoline engines. Therefore, the effects of engine cyclic variability will be most significant for this particle diameter range.

The effect of load on particle size density is embodied in figure 6. It is already known that at a relatively low operating load, most exhaust particles are generally within 10 to 50nm in diameter. Whereas as the load increases for a constant speed, the proportion of small diameter particles decreases as larger diameter particles increase [24,34]. Therefore, the results in figure 6 align with the outcome of similar studies in the literature [24,34]. The particles within the range of 10 - 25 nm diameter have a higher contribution to the total particle count in the 2500 RPM and 20 Nm case in comparison to the 2500 RPM and 80 Nm case. This is expected given that peak cylinder pressure and temperature are higher at high load operating conditions. These combustion parameters have a direct effect on the inception, growth, oxidation and coagulation of nano-scale particles.

This study grouped the particles into different particle size ranges as 5-23, 23-50, 50-100 and 100-300 nm diameter. The particle size ranges were grouped in this manner to align with the chosen particle range grouping in similar studies [34,37,54]. The correlation between these particle size ranges and the total particle count was then examined. The analysis compared the characteristics of these nanoparticle ranges to those of the total signal.

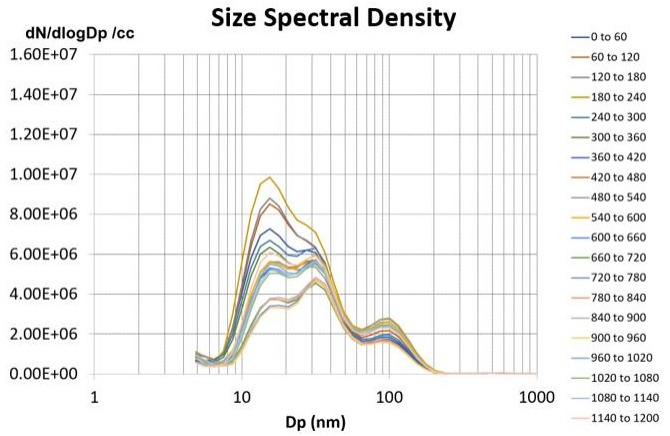

Figure 5: A particle size spectral density plot for every 60 seconds as a function of particle diameter measured upstream of the catalyst at 2500 RPM and 20 Nm operating conditions

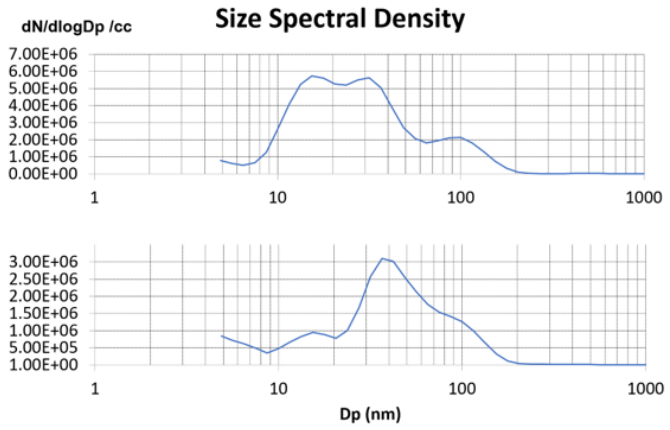

Figure 6: Particle size spectral density measured upstream of the catalyst at a low load case 2500 RPM - 20 Nm (Top figure) and a high load case 2500 RPM - 80 Nm (Bottom Figure)

The resulting particle count measurements used for the analysis are presented as time domain signals. Figure 7 shows an example time domain plot of the total particle count signal ranging from 5 nm to 1000 nm diameter particles measured upstream of the catalyst at 3500 RPM and 20 Nm operating conditions. The measured particle emissions for each operating condition consist of a total time domain

capturing all particles within the 5 nm to 1000 nm diameter range in addition to the specified subgroups of nanoparticle range signals.

EEMD was applied to the time domain data at various operating conditions and IMFs for each speed and load operating conditions were obtained. An example of the resulting IMFs obtained after decomposing the PM measurements in figure 7 is illustrated in figure 8. It can be seen that each obtained IMF contains different oscillations in comparison to the next IMF, with the oscillations frequency decreasing as the IMFs order increases. Therefore, FFT was applied to the IMFs in order to extract the frequency content of these IMFs.

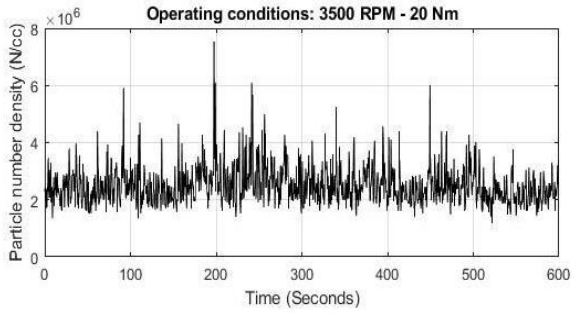

Figure 7: Time domain signal of the total particle count upstream of the catalyst at 3500 RPM – 20 Nm

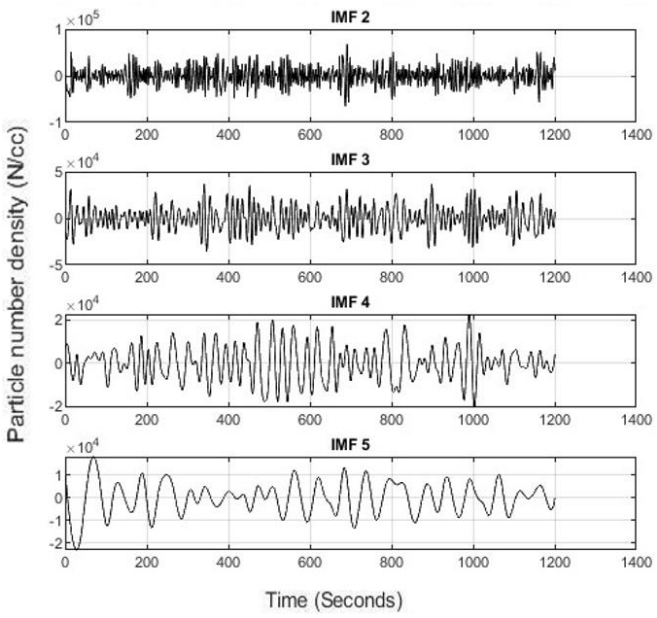

Figure 8: Resulting IMFs 2, 3, 4 and 5 after applying EEMD to the particle density time domain measured upstream of the catalyst at 3500 RPM – 20 Nm

Figures 9 to 14 demonstrate a comparison of the frequency characteristics associated with IMFs 2 to 5 for each nanoparticle range signal and the total PM signal at various operating conditions. The comparison included both pre-catalyst and post-catalyst cases. It can be seen that the fundamental frequency of the total particle count correlates with a different size range as the speed and load change. It is also seen that the frequency of the particle size range that compares favourably with the total particle count for the pre-catalyst is different from that of post-catalyst measurement. For example, figure 9 shows the IMFs fundamental frequency of the specific nanoparticle ranges and the total particle count for the pre-catalyst and post-catalyst at an engine speed of 1500 RPM and 50 Nm loading conditions. In the pre-catalyst case, it can be seen that the fundamental frequency of IMF 2 of the 5-23 nm particle range matches the fundamental frequency of IMF 2 of the total particle count. Similarly, the fundamental frequency of IMF 3 of the 23-50 nm particle range matches the fundamental frequency of IMF 3 of the total particle count. Therefore, it is concluded that the 5-23 nm and 23-50 nm ranges are closely related to the total particle count for the pre-catalyst 1500 RPM and 50 Nm case. In the post-catalyst case, the correlation between IMF 2 of the 5-23 nm particle range and IMF 2 of the total particle count is less prominent. Whereas IMF 3 of the 23-50 nm particle range no longer matches IMF 3 of the total particle count. These observations hence suggest that the three-way catalytic converter affects the particle size spectral density, which reflects on the fundamental frequencies of different particle size ranges.

In contrast, the frequency of 5-23 nm particles closely aligns with the fundamental frequency of total particle count. It has already been shown that the particle number density around 10nm diameter after the catalytic converter usually drops when compared to Pre-Catalyst values [53]. Whereas the particle number density around 100 nm diameter after the catalytic converter increases when compared to the Pre-catalyst values. EEMD provides an insight into the correlation between the 5-23 nm particle range and the total particle count. Similarly, EEMD provides insight into the influence of the catalytic converter on particulate matter emissions.

Figure 10 shows the effect of load on particle size and count. As the load increases from 50 to 80 Nm, the correlation between all IMFs of the 23-50 nm particles with the IMFs of the total particle count of the pre-catalyst sample is more significant. For the post-catalyst case, the IMFs frequencies of 100-300 nm particles compare favourably with the IMFs of the total particle count. These findings align well with the background literature. Increasing the load results in a decrease of smaller particles [24,34] and therefore a less significant correlation between the 5-23 nm particles and the total particle count signal at 1500 RPM – 80 Nm in comparison to the 1500 RPM – 50 Nm case. Similarly, it was shown that three-way catalytic converters can influence the particle size distribution characteristics and result in an increased number of larger diameter particles [53]. This explains the strong correlation between the 100-300 nm particles and the total particle count signal in the post-catalyst case in figure 10.

The frequency characteristics derived from IMFs for the 2500 RPM – 20 Nm and 2500 RPM - 50 Nm cases are shown in figures 11 and 12, respectively. Whereas the frequency characteristics derived from IMFs for the 3500 RPM – 20 Nm and 3500 RPM - 80 Nm cases are shown in figures 13 and 14, respectively. Overall, it was found that IMF 2 of the 5-23 nm particle spectrum and IMF 2 of total particle count were correlated for 83% of the pre-catalyst testing cases. Whereas this correlation was less prominent in the post-catalyst cases. The effect of load for the other operating speeds also agrees with the conclusion drawn from the 1500 RPM case. The effect of engine load on particle emissions is more dominant in comparison to the effect of speed given the direct relation between load settings and in-cylinder combustion

conditions. The analysis performed during the present work was limited to the speed range of 1500 RPM to 3500 RPM and a load range of 20 Nm to 80 Nm. However, further EEMD-FFT analysis of particulate matter data from a wider range of speed and load operating conditions could further validate the findings of this work and reveal additional correlations between the nanoparticle ranges and the total particle count.

The application of EEMD and IMFs provides a useful insight into inter-particle correlations and their effect on the total particle count for the pre-catalyst and post-catalyst measurements. Therefore, such information can provide a practical input for developing suitable strategies to control particle emissions as well as predicting the effect of a catalytic converter design on particle size characteristics. The EEMD-FFT approach highlighted in the present work can also be combined with other mathematical methods in the literature to facilitate its implementation in a control algorithm. For example, the work performed by El Yacoubi and Samuel in [49] identified the presence of a frequency coupling between cylinder pressure, manifold pressure and the crankshaft instantaneous speed signal using bispectral analysis. Given that the EEMD-FFT method used in the present work is capable of extracting the frequency characteristics of the decomposed PM data, it is possible to combine this method with bispectral analysis to extract potential frequency couplings between the IMFs of PM data and other signals such as cylinder pressure. Such coupling can be used in common engine calibration models such as mean value engine models (MVEM) for particulate matter emissions control purposes.

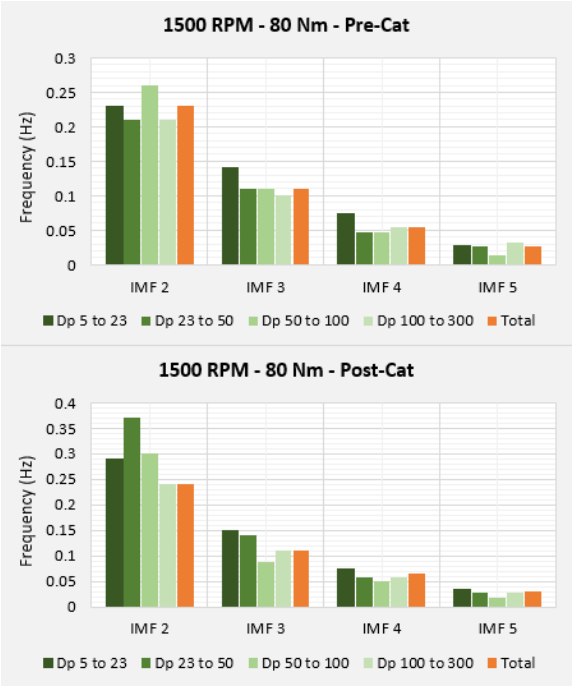

Figure 10: A comparison of the total PM signal IMFs with the IMFs of specific nanoparticle ranges at 1500 RPM and 80 Nm. The comparison includes a pre-catalyst case (Top bar chart) and a post-catalyst case (Bottom bar chart)

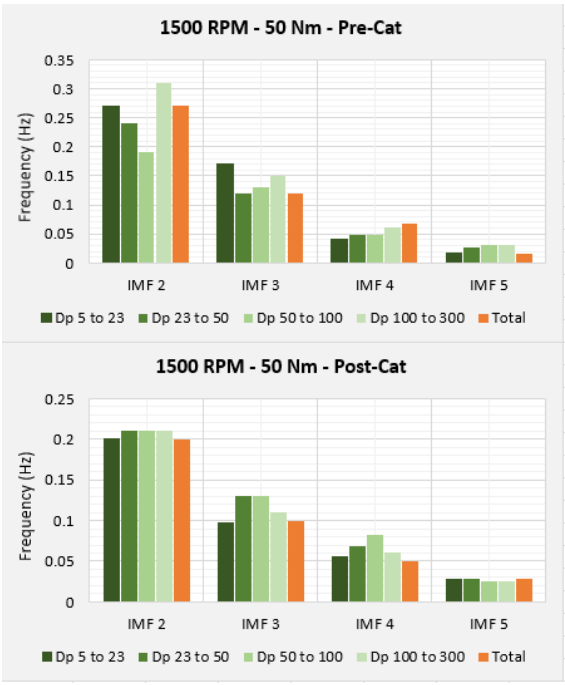

Figure 9: A comparison of the total PM signal IMFs with the IMFs of specific nanoparticle ranges at 1500 RPM and 50 Nm. The comparison includes a pre-catalyst case (Top bar chart) and a post-catalyst case (Bottom bar chart)

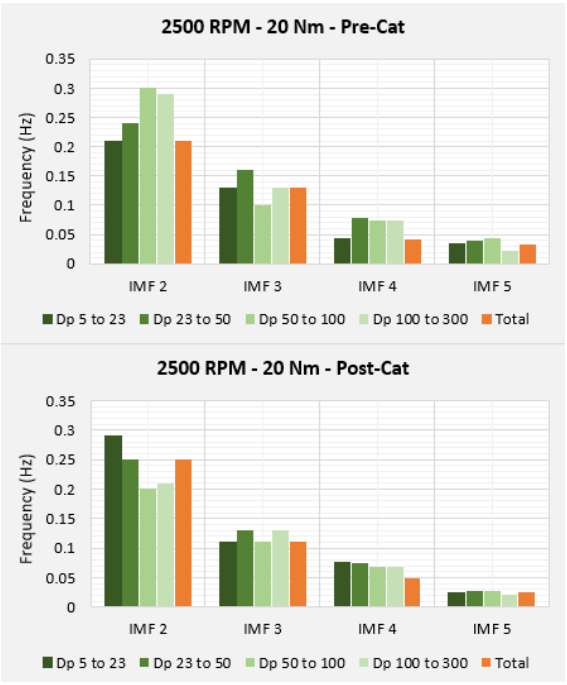

Figure 11: A comparison of the total PM signal IMFs with the IMFs of specific nanoparticle ranges at 2500 RPM and 20 Nm. The comparison includes a pre-catalyst case (Top bar chart) and a post-catalyst case (Bottom bar chart)

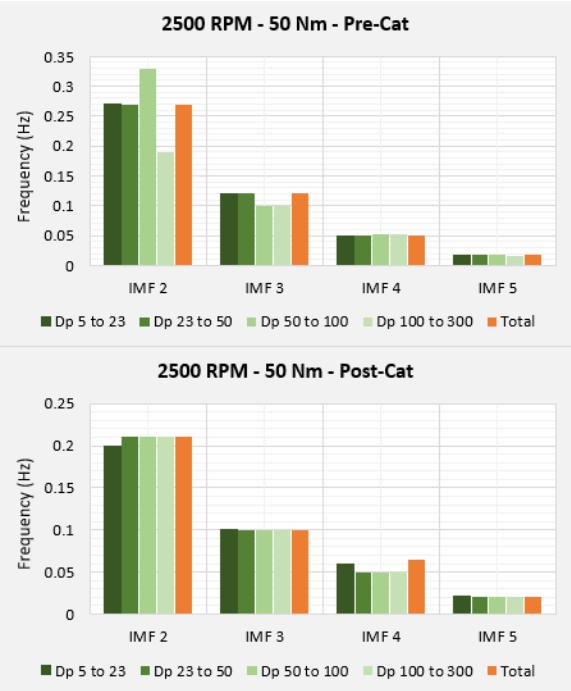

Figure 12: A comparison of the total PM signal IMFs with the IMFs of specific nanoparticle ranges at 2500 RPM and 50 Nm. The comparison includes a pre-catalyst case (Top bar chart) and a post-catalyst case (Bottom bar chart)

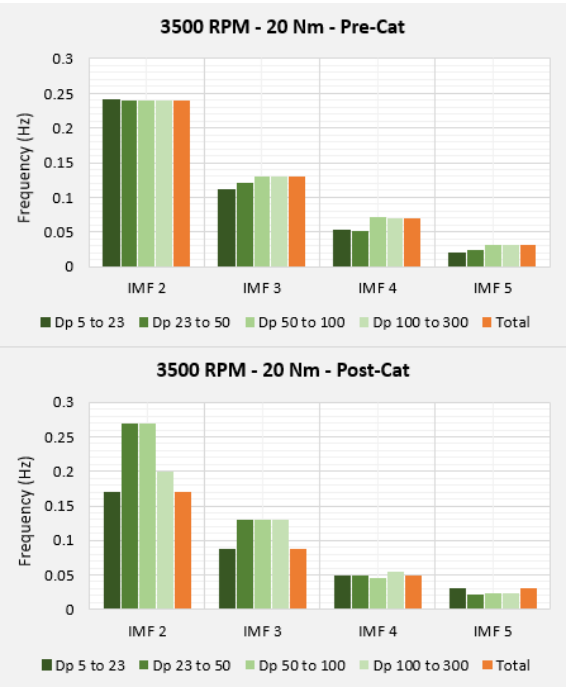

Figure 13: A comparison of the total PM signal IMFs with the IMFs of specific nanoparticle ranges at 3500 RPM and 20 Nm. The comparison includes a pre-catalyst case (Top bar chart) and a post-catalyst case (Bottom bar chart)

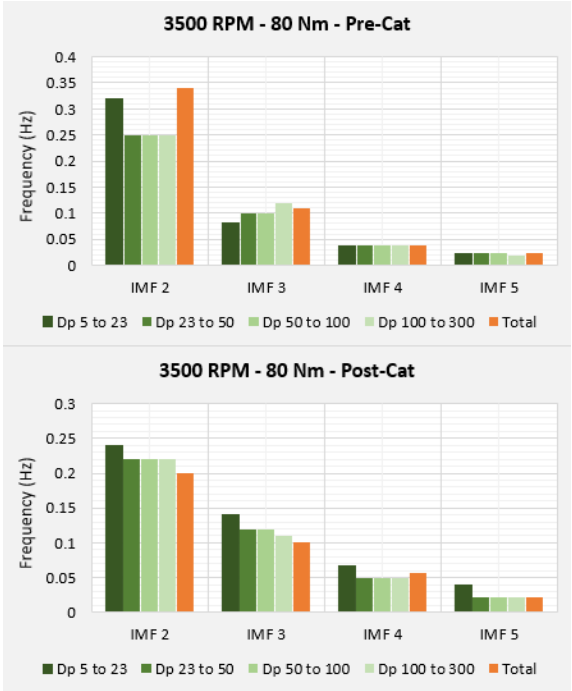

Figure 14: A comparison of the total PM signal IMFs with the IMFs of specific nanoparticle ranges at 3500 RPM and 80 Nm. The comparison includes a pre-catalyst case (Top bar chart) and a post-catalyst case (Bottom bar chart)

Conclusions

The present work introduces a systematic approach to analyse particulate matter data from a 4-stroke, 4-cylinder, 1.6 Litre, spark ignition, gasoline direct injection engine using an EEMD-FFT method. The application of EEMD as a tool for examining the correlation between different particle size ranges and the total particle count has highlighted that at a relatively low operating load, IMF 2 of the 5-23 nm particle spectrum and IMF 2 of total particle count were correlated for 83% of the pre-catalyst testing cases. Similarly, as the load increases the fundamental frequency of the 23-50 nm particles tends to correlate with the total particle count. The present work focused on analysing particulate matter emissions data associated with a speed range of 1500 RPM to 3500 RPM and a load range of 20 Nm to 80 Nm. However, further EEMD-FFT analysis of PM data from a wider range of operating conditions could reveal additional correlations between the nanoparticle ranges and the total particle count. Additionally, the use of EEMD in the present work also showed that the three-way catalytic converter altered the effect of certain nanoparticle ranges on the total particle count signal.

The findings of this work can provide a useful insight for developing a control strategy to be embedded in engine calibration models such as mean value engine models for controlling particulate matter emissions. Whereas the findings related to the effect of the three-way catalytic converter on PM emissions can also be used as a reference during the design and evaluation process of gasoline after-treatment systems.

References

1. Qian, Y., Li, Z., Yu, L., Wang, X., et al., "Review of the state-of-the-art of particulate matter emissions from modern gasoline fueled engines," *Applied Energy* 238 (2019): 1269-1298, doi: 10.1016/j.apenergy.2019.01.179.

2. Raza, M., Chen, L., Leach, F., and Ding, S., "A review of particulate number (PN) emissions from gasoline direct injection (GDI) engines and their control techniques," *Energies* 11 (2018): 1417, doi: 10.3390/en11061417.

3. Kittelson, D., "Engines and nanoparticles: a review," *Journal of aerosol science* 29 (1998): 575-588, doi: 10.1016/S0021-8502(97)10037.

4. Leach, F ., Chapman, E ., Jetter, J ., Rubino, L., et al., "A Review and Perspective on Particulate Matter Indices Linking Fuel Composition to Particulate Emissions from Gasoline Engines," *SAE Int. J. Fuels Lubr.* 15 (1) : 3 – 28, 2022, doi: 10.4271/04-15-01-0001.

5. Richter, H., and Howard, J., "Formation of polycyclic aromatic hydrocarbons and their growth to soot—a review of chemical reaction pathways," *Progress in Energy and Combustion science* 26 (2000): 565-608, doi: 10.1016/S0360-1285(00)00009-5.

6. Giechaskiel, B., Joshi, A., Ntziachristos, L., and Dilara, P., "European regulatory framework and particulate matter emissions of gasoline light-duty vehicles: A review," *Catalysts* 9 (2019): 586, doi: 10.3390/catal9070586.

7. Ariztegui, J., Barsch, T., Carbone, R., Carbonas, A., et al., "Gasoline Direct Injection Particulate Study," https://www.concawe.eu/wp-content/uploads/2017/01/rpt_16-10.pdf, Accessed June. 2023.

8. Haynes, B., and Wagner, H., "Soot formation.," *Progress in energy and combustion science* 7 (1981): 229-273, doi: 10.1016/0360-1285(81)90001-0.

9. Amann, C., and Siegla, D., "Diesel particulates—what they are and why," Aerosol *Science and Technology* 1 (1982): 73-101, doi: 10.1080/02786828208958580.

10. Heywood, J., *Internal Combustion Engine Fundamentals*, 1st ed. (New York [etc.]: McGraw-Hill, 1988), 1-10, ISBN: 0-07-028637-X.

11. Linsinger, T., Roebben, G., Gilliland, D., Calzolai, L., et al., "Requirements on measurements for the implementation of the European Commission definition of the term `nanomaterial`," EUR 25404 EN, Luxembourg, July, 2012.

12. Price, P., Stone, R., Collier, T., Davies, M. et al., "Dynamic Particulate Measurements from a DISI Vehicle: A Comparison of DMS500, ELPI, CPC and PASS," SAE Technical Paper 2006-01-1077, 2006, doi: 10.4271/2006-01-1077.

13. Oberdörster, G., Oberdörster, E., Oberdörster, J., "Nanotoxicology: an emerging discipline evolving from studies of ultrafine particles," *Environmental health perspectives* 113 (2005): 823-839, doi: 10.1289/ehp.7339.

14. Frenklach, M., and Warnatz, J., "Detailed modeling of PAH profiles in a sooting low-pressure acetylene flame," *Combustion science and technology* 51 (1987): 265-283, doi: 10.1080/00102208708960325.

15. Melius, C., Colvin, M., Marinov, N., Pitz, W., et al., "Reaction mechanisms in aromatic hydrocarbon formation involving the C5H5 cyclopentadienyl moiety," *Symposium (International) on Combustion* 26 (1996): 685-692, doi: 10.1016/S0082-0784(96)80276-1.

16. Frenklach, M., and Mebel, A., "On the mechanism of soot nucleation," *Physical Chemistry Chemical Physics* 22 (2020): 5314-5331, doi: 10.1039/D0CP00116C.

17. Nicovich, J., Ravishankara, A., "Reaction of hydrogen atom with benzene: kinetics and mechanism," *The Journal of Physical Chemistry* 88 (1984): 2534-2541, doi: 10.1021/j150656a021.

18. Mebel, A., Lin, M., Yu, T., and Morokuma, K., "Theoretical study of potential energy surface and thermal rate constants for the C6H5+ H2 and C6H6+ H reactions," *The Journal of Physical Chemistry A* 101 (1997): 3189-3196, doi: 10.1021/jp9702356.

19. Etikyala, S., Koopmans, L., and Dahlander, P., "History Effect on Particulate Emissions in a Gasoline Direct Injection Engine," *SAE Int. J. Engines* 15(3): 445-455, 2022, doi: 10.4271/03-15-03-0999.

20. Whitaker, P., Kapus, P., Ogris, M., and Hollerer, P., "Measures to Reduce Particulate Emissions from Gasoline DI engines," *SAE Int. J. Engines* 4(1): 1498-1512, 2011, doi: 10.4271/2011-01-1219.

21. Petit, B., Boiarciuc, A., Radenac, E., Delahaye, L., et al., "PN Formation Mechanism and Countermeasures with the Spray Design on Port Fuel InjectionSI Engine," SAE Technical Paper 2018-01-1417, 2018, doi: 10.4271/2018-01-1417.

22. Papagiannakis, R., Rakopoulos, D., and Rakopoulos, C., "Theoretical study of the effects of spark timing on the performance and emissions of a light-duty spark ignited engine running under either gasoline or ethanol or butanol fuel operating modes," *Energies* 10 (2017):1198, doi: 10.3390/en10081198.

23. Schueck, C., Koch, T., Samenfink, W., Schuenemann, E., et al., "Optical Investigations of Soot Formation Mechanisms and Possible Countermeasures on a Turbocharged Port Fuel Injection SI Engine," *SAE Int. J. Engines* 9(4): 2010-2021, 2016, doi: 10.4271/2016-01-2163.

24. Whelan, I., Samuel, S., Timoney, D., and Hassaneen, A., "Characteristics of Nano-Scale Particulates from Gasoline Turbo-Intercooled Direct-Injection Engine," *SAE Int. J. Fuels Lubr.* 3(2): 839-848, 2010, doi: 10.4271/2010-01-2197.

25. Hochhauser, A., Schleyer, C., Yeh, L., and Rickeard, D., "Impact of Fuel Sulfur on Gasoline and Diesel Vehicle Emissions," SAE

Technical Paper 2006-01-3370, 2006, doi: 10.4271/2006-01-3370.

26. Maier, A., Klaus, U., Dreizler, A., and Rottengruber, H., "Fuel-Independent Particulate Emissions in an SIDI Engine," *SAE Int. J. Engines* 8(3): 1334-1341, 2015, doi: 10.4271/2015-01-1081.

27. Hall, D. and Dickens, C., "The Effect of Sulphur-Free Diesel Fuel on the Measurement of the Number and Size Distribution of Particles Emitted from a Heavy-Duty Diesel Engine Equipped with a Catalysed Particulate Filter," SAE Technical Paper 2003-01-3167, 2003, doi: 10.4271/2003-01-3167.

28. Zhang, Q., Fang, J., Meng, Z., Chen, C., et al., "Thermogravimetric analysis of soot combustion in the presence of ash and soluble organic fraction," *RSC advances* 10 (2020): 33436-33443, doi: 10.1039/D0RA06384C.

29. Seong, H., Choi, S., and Lee, K., "Examination of nanoparticles from gasoline direct-injection (GDI) engines using transmission electron microscopy (TEM)," International Journal of Automotive Technology 15 (2014): 175-181, doi: 10.1007/s12239-014-0019-5.

30. Lance, M., Toops, T., Moses-DeBusk, M., Kaul, B., et al., "Investigation of Lubricant Additive Interactions on Gasoline Particulate Filters," *SAE Int. J. Fuels Lubr.* 16(3): 2023.

31. Andersson, J., and Giechaskiel, B., "Munoz Bueno R, Sandbach E, Dilara P. Particle Measurement Programme (PMP) Light-duty Inter-laboratory Correlation Exercise (ILCE_LD) Final Report," EUR 22775 EN, Italy, June, 2007.

32. Terres, A., Ebert, V., Nowak, A., Rosahl, J., et al., "Particle Measurement Programme (PMP): Inter-laboratory correlation exercise with Condensation Particle Counters (CPCs)," EUR 29277 EN, Luxembourg, Italy, 2018.

33. Cucchi, M., and Samuel, S., "Influence of the exhaust gas turbocharger on nano-scale particulate matter emissions from a GDI spark ignition engine," *Applied Thermal Engineering* 76 (2015): 167-174, doi: 10.1016/j.applthermaleng.2014.11.002.

34. Whelan, I., Timoney, D., Smith, W., and Samuel, S., "The Effect of a Three-Way Catalytic Converter on Particulate Matter from a Gasoline Direct-Injection Engine During Cold-Start," *SAE Int. J. Engines* 6(2):1035-1045, 2013, doi: 10.4271/2013-01-1305.

35. Boger, T., Glasson, T., Rose, D., Ingram-Ogunwumi, R., et al., "Next Generation Gasoline Particulate Filters for Uncatalyzed Applications and Lowest Particulate Emissions," *SAE Int. J. Advances & Curr. Prac. in Mobility* 3(5): 2452-2461, 2021, doi: 10.4271/2021-01-0584.

36. Liu, H., Li, Z., Xu, H., Ma, X., et al., "Nucleation mode particle evolution in a gasoline direct injection engine with/without a three-way catalyst converter," *Applied Energy* 259 (2020): 114211, doi: 10.1016/j.apenergy.2019.114211.

37. Samuel, S., Hassaneen, A., and Morrey, D., "Particulate Matter Emissions and the Role of Catalytic Converter During Cold Start of GDI Engine," SAE Technical Paper 2010-01-2122, 2010, doi:10.4271/2010-01-2122.

38. Cucchi, M., and Samuel, S., "Application of the Lambert W function for the impact of the exhaust gas turbocharger on nanoscale PM emissions from a TGDI engine," *Applied Thermal Engineering* 99 (2016): 429-433, doi: 10.1016/j.applthermaleng.2015.12.125.

39. Yamaguchi, A., Dillner, J., Helmantel, A., Koopmans, L. et al., "Ultra-High Fuel Pressure in GDI to Suppress Particulate Formation during Warming-Up and Load Transients," SAE Technical Paper 2023-01-0239, 2023, doi: 10.4271/2023-01-0239.

40. Ketterer, J., "Soot Formation in Direct Injection Spark Ignition Engines Under Cold-Idle Operating Conditions," Ph.D. Thesis, MIT, 2013.

41. Anbari Attar, M., and Xu, H., "Correlations between particulate matter emissions and gasoline direct injection spray characteristics," *J. Aerosol Science* 102 (2016): 128-141, doi: 10.1016/j.jaerosci.2016.09.006.

42. Wang, X., Chen, W., Huang, Y., Wang, L., et al., "Advances in soot particles from gasoline direct injection engines: A focus on physical and chemical characterisation," *Chemosphere* 311 (2022): 137181, doi: 10.1016/j.chemosphere.2022.137181.

43. Piock, W., Hoffmann, G., Berndorfer, A., Salemi, P. et al., "Strategies Towards Meeting Future Particulate Matter Emission Requirements in Homogeneous Gasoline Direct Injection Engines," *SAE Int. J. Engines* 4(1): 1455-1468, 2011, doi: 10.4271/2011-01-1212.

44. Wu, Z., and Huang, N., "Ensemble Empirical Mode Decomposition: A Noise-Assisted Data Analysis Method," *World Scientific* 1 no. 1 (2009): 1-41, doi: 10.1142/S1793536909000047.

45. Gaci, S., "A New Ensemble Empirical Mode Decomposition (EEMD) Denoising Method for Seismic Signals," *Energy Procedia* 97 (2016): 85-91, doi: 10.1016/j.egypro.2016.10.026.

46. Huang, N., Shen, Z., Long, S., Wu, M., et al., "The Empirical Mode Decomposition and the Hilbert Spectrum for Nonlinear and Non-Stationary Time Series Analysis", *the Royal Society Publishing* 454 (1971): 903-995, doi: 10.1098/rspa.1998.0193.

47. Wang, L., and Shao, Y., "Fault feature extraction of rotating machinery using a reweighted complete ensemble empirical mode decomposition with adaptive noise and demodulation analysis," *Mechanical systems and signal processing* 138 (2020): 106545, doi: 10.1016/j.ymssp.2019.106545.

48. Park, S., Kim, S., and Choi, J., "Gear fault diagnosis using transmission error and ensemble empirical mode decomposition," *Mechanical Systems and Signal Processing* 108 (2018): 262-275, doi: 10.1016/j.ymssp.2018.02.028.

49. El Yacoubi, I. and Samuel, S., "Frequency Coupling Analysis in Spark Ignition Engine Using Bispectral Method and Ensemble Empirical Mode Decomposition," SAE Technical Paper 2022-01-0481, 2022, doi:10.4271/2022-01-0481.

50. Lee, Z., Kim, D., and Park, S., "Effects of spray behavior and wall impingement on particulate matter emissions in a direct injection spark ignition engine equipped with a high pressure injection system," *Energy Conversion and Management* 213 (2020): 112865, doi: 10.1016/j.enconman.2020.112865.

51. Leach, F., Stone, R., Fennell, D., Hayden, D., et al., "Predicting the particulate matter emissions from spray-guided gasoline direct-injection spark ignition engines," *Proceedings of the Institution of Mechanical Engineers, Part D: Journal of Automobile Engineering* 231 (2017): 717-730, doi: 10.1177/0954407016657453.

52. Zhang, M., Hong, W., Xie, F., Su, Y., et al., "Combustion, performance and particulate matter emissions analysis of operating parameters on a GDI engine by traditional experimental investigation and Taguchi method," *Energy Conversion and Management* 164 (2018): 344-352, doi: 10.1016/j.enconman.2018.03.017.

53. Whelan, I., Samuel, S., and Hassaneen, A., "Investigation into the Role of Catalytic Converters on Tailpipe-out Nano-Scale Particulate Matter from Gasoline Direct Injection Engine," SAE Technical Paper 2010-01-1572, 2010, doi:10.4271/2010-01-1572.

54. Whelan, I., Smith, W., Timoney, D., and Samuel, S., "The Effect of Engine Operating Conditions on Engine-out Particulate Matter from a Gasoline Direct-injection Engine during Cold-start.," SAE Technical Paper 2012-01-1711, 2012, doi:10.4271/2012-01-1711.

Definitions/Abbreviations

PM	Particulate Matter
GDI	Gasoline Direct Injection
GPF	Gasoline particulate filter
PAH	Polycyclic Aromatic Hydrocarbons
EEMD	Ensemble Empirical Mode Decomposition
IMF	Intrinsic Mode Function
NADA	Noise-assisted data analysis
EMD	Empirical Mode Decomposition
FFT	Fast Fourier Transform
WGDI	Wall guided direct injection
ECU	Engine Control Unit
DMS	Differential Mobility Spectrometer
GMD	Geometric Mean Diameter
IDE	Integrated development environment
MVEM	Mean value engine model